Structural Differences of Bacterial and Mammalian K$^+$ Channels*

Anja Wrisch and Stephan Grissmer‡

From the Department of Applied Physiology, University of Ulm, Albert-Einstein-Allee 11, 89081 Ulm, Germany

Using a peptide toxin, kaliotoxin (KTX), we gained new insight into the topology of the pore region of a voltage-gated potassium channel, *m*Kv1.1. In order to find new interactions between *m*Kv1.1 and KTX, we investigated the pH dependence of KTX block which was stronger at pH$_o$ 6.2 compared with pH$_o$ 7.4. Using site-directed mutagenesis on the channel and the toxin, we found that protonation of His^{34} in KTX caused the pH$_o$ dependence of KTX block. Glu^{350} and Glu^{353} in *m*Kv1.1, which interact with His^{34} in KTX, were calculated to be 4 and 7 Å away from His^{34}/KTX, respectively. Docking of KTX into a homology model of *m*Kv1.1 based on the *KcsA* crystal structure using this and other known interactions as constraints showed structural differences between *m*Kv1.1 and *KcsA* within the turret (amino acids 348–357). To satisfy our data, we would have to modify the *KcsA* crystal structure for the *m*Kv1.1 channel orienting Glu^{350} 7 Å and Glu^{353} 4 Å more toward the center of the pore compared with *KcsA*. This would place Glu^{350} 15 Å and Glu^{353} 11 Å away from the center of the pore instead of the distances for the equivalent *KcsA* residues with 22 Å for Gly^{53} and 15 Å for Gly^{56}, respectively. Bacterial and mammalian potassium channels may have structural differences regarding the turret of the outer pore vestibule. This topological difference between both channel types may have substantial influence on structure-guided development of new drugs for mammalian potassium channels by rational drug design.

Voltage-gated potassium channels guide fundamental biological processes such as electrical signaling, osmotic balance and signal transduction (1). Peptide toxins from scorpions, snakes, and sea anemones, which inhibit ion conduction through potassium channels by binding within the outer pore region, have been used to characterize physiological significance, localization, and structural aspects of these channels (2). Charybdotoxin (CTX)[1] has been used to characterize the region of potassium channels bearing both the CTX receptor and the ion conduction pathway and to demonstrate the tetrameric stoichiometry of the channel (3, 4). Estimations of the topology of the external vestibule of various potassium channels were successful because the structure of the peptide toxins, which

was structurally defined by NMR studies, reports the complementary shape of the binding partner (5, 6). Structural features of different channel types were announced by specific binding properties of peptide toxins (7). Our knowledge about structural characteristics of potassium channels was confirmed and extended through data from the bacterial *Streptomyces KcsA* channel based on crystallographic studies (8). Therefore, up to the availability of x-ray data for each potassium channel, further application of peptide toxins as molecular calipers to investigate the architecture of structurally non-defined targets appears to be reasonable.

Several toxins display a blocking affinity dependent on the extracellular pH (pH$_o$) but until now only a decreased block at acid pH$_o$ was known; both with peptide toxins (9–11) and with other blockers working on potassium channels like TEA (12) but also working on sodium channels like tetrodotoxin and saxitoxin (13). The reduced CTX affinity of the F425H mutant *Shaker* channel and of the wt Kv1.3 channel (9, 11) as well as the lowered TEA affinity of *m*Kv1.1 channels (12) at low pH$_o$ was caused by protonation of histidine residues within the outer vestibule of the respective channel proteins. Affinity of tityustoxin to the squid Kv1 channel SqKv1A, which contains a histidine at *Shaker* position 425, is also reduced at acid pH$_o$ (14). In contrast, in *m*Kv1.1 and H404T mutant *m*Kv1.3 channels, we observed a better KTX block at low pH$_o$. In this paper we present evidence that protonation of a histidine in KTX, which interacts with negatively charged amino acids in the outer pore region of *m*Kv1.1 and H404T mutant *m*Kv1.3 channels, is responsible for the higher KTX affinity of these channels. Using electrostatic compliance we found distances of 4 and 7 Å between Glu^{353} and Glu^{350} in *m*Kv1.1 and His^{34} in KTX, respectively. Our data define the position of the turret (amino acids 348–357) in Kv1.1 and also Kv1.3 and imply structural differences between mammalian and bacterial K$^+$ channels in that region. These results help refine our picture of the spatial arrangement of amino acid residues in the outer pore region of Kv1.1 and Kv1.3 that might facilitate therapeutic drug design.

MATERIALS AND METHODS

Cells—All experiments were carried out on single cells of a rat basophilic leukemia cell line, RBL cells (15). Cells were obtained from the American Type Culture Collection (Rockville, MD). The cells were maintained in a culture medium of Minimal Essential Medium with Earle's salts supplemented with 1 mM L-glutamine and 10% heat-inactivated fetal calf serum in a humidified, 5% CO$_2$ incubator at 37 °C. Cells were plated to grow non-confluently onto glass 1 day prior to use for injection and electrophysiological experiments (16).

Solutions—The experiments were done at room temperature (21–25 °C). Cells measured in the whole cell configuration were normally bathed in mammalian Ringer's solution containing, in mM: 160 NaCl, 4.5 KCl, 2 CaCl$_2$, 1 MgCl$_2$, and 10 *X* (with *X* either Tris, HEPES, MES, or citrate), with an osmolarity of 290–320 mOsm. The pH was adjusted to 5.5, 6.2 (*X*: citrate); to 6.2, 6.6, 6.8, 7.0 (*X*: MES), and to 7.0, 7.4, 7.8 (*X*: HEPES), and to 7.8, 8.2 (*X*: Tris) with NaOH. No differences in current were seen comparing mammalian Ringer's solution containing either citrate or MES at pH$_o$ 6.2, either MES or HEPES at pH$_o$ 7.0, and either

[1] The abbreviations used are: CTX, charybdotoxin; Dab, diaminobutyric acid; Dap, diaminopropionic acid; KTX, kaliotoxin; KTX$_3$, kaliotoxin 3; NTX, noxiustoxin; pH$_o$, extracellular pH; ThLys, thiohomolysine; wt, wild type; TEA, tetraethylammonium; MES, 4-morpholineethanesulfonic acid; FITC, fluorescein isothiocyanate; Ω, ohm(s); S, siemen(s).

Mammalian K$^+$ Channel Structure

HEPES or Tris at pH$_o$ 7.8 as described earlier (12). A simple syringe-driven perfusion system was used to exchange the bath solutions in the recording chamber. The internal pipette solution for the whole-cell recordings contained (in mM): 155 KF, 2 MgCl$_2$, 10 HEPES, 10 EGTA, adjusted to pH 7.2 with KOH, with an osmolarity of 290–320 mOsm.

Toxins—Kaliotoxin was purchased from Bachem Biochemica GmbH (Heidelberg, Germany) or made by recombinant methods (see below). Because of different batches of KTX, KTX from only one charge was used in each experiment. CTX was obtained from Bachem Biochemica GmbH (Heidelberg, Germany). Noxiustoxin (NTX) was a generous gift from Dr. Stephen Brady (Merck Institute, West Point, PA). The Lys^{27} mutants of KTX (K27Dap, K27Dab, K27Nle, K27ThLys, K27A) were generous gifts from Dr. K. George Chandy (University of California, Irvine, CA). KTX$_3$ was kindly provided by Dr. Martin-Eauclaire (Marseille, France). KTX mutants H34A, H34K, R31A/H34A, and K32A were generated recombinantly with friendly help of Dr. H. G. Knaus and Maria Trieb at the Department of Biochemical Pharmacology (University of Innsbruck, Innsbruck, Austria) (17).

The lyophilized peptides were stored at −70 °C. Stock solutions of 10–100 μM were made with mammalian Ringer's solution containing 0.1% bovine serum albumin. The final dilutions were prepared shortly before the experiment.

Electrophysiology—Experiments were carried out using the whole-cell recording mode of the patch-clamp technique as described before (16). Electrodes were pulled from glass capillaries (Clark Electromedical Instruments, Reading, United Kingdom) in three stages, coated with Sylgard (Dow Corning, Seneffe, Belgium), and fire-polished to resistances measured in the bath of 2.5–4 MΩ. Membrane currents were recorded with an EPC-9 patch-clamp amplifier (HEKA Elektronik, Lambrecht, Germany) interfaced to a Macintosh computer running acquisition and analysis software (Pulse and PulseFit). Capacitative and leak currents were subtracted using the P/10 procedure. Series resistance compensation (>80%) was employed if the current exceeded 1 nA. The holding potential in all experiments was −80 mV.

Expression—pBSTA plasmids containing the entire coding sequence of the *m*Kv1.1 wild type (wt) gene, and the pSP64T plasmids containing the sequences for the H404T mutant *m*Kv1.3 channel (18) (a generous gift from Dr. K. George Chandy) were linearized with *Pst*I and *Eco*RI, respectively and *in vitro* transcribed with the T7 (*m*Kv1.1) and SP6 (*m*Kv1.3 H404T) Cap-Scribe system (Roche Molecular Biochemicals). The resulting cRNA was phenol/chloroform-purified and could be stored at −75 °C for several months.

Injection—The cRNA was diluted with a fluorescent FITC dye (0.5% FITC-dextran in 100 mM KCl) to a final concentration of 1 μg/μl. RBL cells were injected with the cRNA/FITC solution filled in injection capillaries (Femtotips$^®$) using an Eppendorf microinjection system (Micromanipulator 5171 and Transjector 5246). In the visualized cells, specific currents could be measured 3–6 h after injection.

Mutagenesis—All mutants of *m*Kv1.1, *m*Kv1.3, and KTX were generated by using the QuikChange^{TM} site-directed mutagenesis kit (Stratagene, Heidelberg, Germany). Mutations were confirmed by sequencing plasmid DNA with the Cy5-AutoRead kit (Amersham Pharmacia Biotech, Uppsala, Sweden).

Thermodynamic Mutant Cycle Analysis—Thermodynamic mutant cycles assist in studying of coupling energies between pairs of amino acid in a protein-protein complex. The dimensionless Ω value, which indicates the interaction strength of a given channel-toxin pair, was calculated as shown before (9, 19). The change in coupling energy, ΔΔG, for the channel-toxin pairs was calculated using the formula $\Delta\Delta G = kT \ln\Omega$ as described earlier (7). The distances between this pair of residues was estimated based on the studies of Schreiber and Fersht (20) and Hidalgo and MacKinnon (19), assuming that ΔΔG values ≥0.5 kcal mol^{-1} correspond to an inter-residue distance of ≤5 Å.

Electrostatic Compliance Measurements—For the estimation of the distances between the charges at KTX position His^{34} and positions Glu^{350} and Glu^{353} in the *m*Kv1.1 channel (equivalent to Asp^{375} and Ser^{378} in *m*Kv1.3), we used the method of electrostatic compliance (5, 9, 12). Protonation of His^{34} in KTX creates a higher effective KTX concentration at the receptor site of the channels compared with the bulk concentration. Calculation of the potential ψ causing the higher effective KTX concentration and the appropriate distances between the interacting amino acids was performed as described by Bretschneider *et al.* (12).

Docking—KTX was docked into a homology model of *m*Kv1.1 based on the x-ray data of the *KcsA* channel. To create a homology model of *m*Kv1.1, we exchanged the *KcsA* amino acids with the equivalent *m*Kv1.1 sequence. Using the *KcsA* structure as template (Protein Data Bank code 1BL8; Ref. 8), we calculated the *m*Kv1.1 homology structure
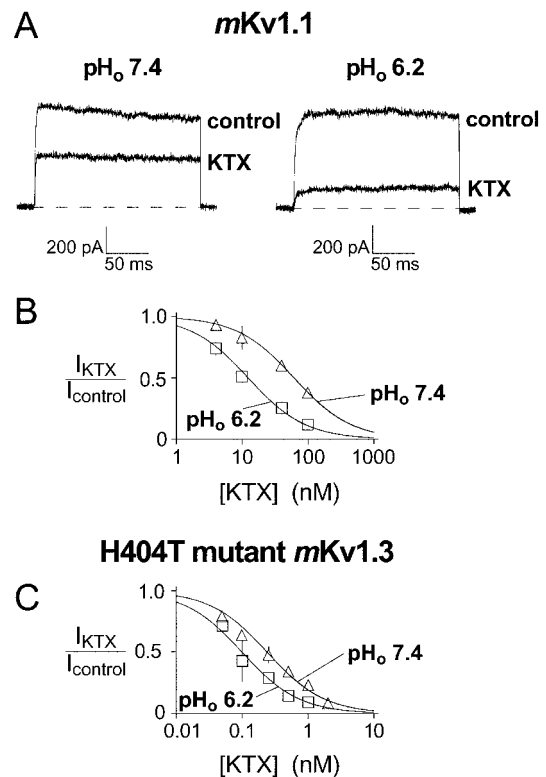
FIG. 1. **Effect of extracellularly applied KTX on currents through *m*Kv1.1 and H404T mutant *m*Kv1.3 channels.** *A*, pH$_o$-dependent KTX block of *m*Kv1.1 channels. Currents were elicited by 200 ms depolarizing voltage steps from a holding potential of −80 mV to +40 mV every 20 s at pH$_o$ 7.4 and 6.2, respectively. Currents were recorded before (control) and after external application of 60 nM KTX. The applied KTX was purchased from Bachem. *B*, dose-response curve for KTX to block peak current through *m*Kv1.1 channels at pH$_o$ 7.4 (△) and pH$_o$ 6.2 (□). *Data points*, peak currents elicited as in *A* (*top*) in the presence of different KTX concentrations (I_{KTX}) were divided by the peak currents without KTX ($I_{control}$). Ratios $I_{KTX}/I_{control}$ of at least four independent experiments are shown as mean ± standard deviation (*error bars* are only shown if they exceed the size of the symbol) and plotted against the indicated KTX concentration. The lines through the points were fitted to a modified Hill equation ($I_{toxin}/I_{control} = 1/[1 + ([toxin]/K_d)]$) with a Hill coefficient of 1 revealing a K_d of 62 nM at pH$_o$ 7.4 and of 19 nM at pH$_o$ 6.2, respectively. *C*, dose-response curve for KTX to block peak current through H404T/*m*Kv1.3 channels at pH$_o$ 7.4 (△) and pH$_o$ 6.2 (□). The fit was made as described in *B*, indicating a K_d of 0.24 nM at pH$_o$ 7.4 and of 0.10 nM at pH$_o$ 6.2, respectively. The applied KTX was purchased from Bachem.

as described before (7). The protein backbone of the *m*Kv1.1 homology model was identical to the *KcsA* backbone. Docking of KTX into the *m*Kv1.1 homology model was performed using the interactions between *m*Kv1.1 and KTX as described before (7, 21). Additionally, the well characterized interaction between the terminal amino group of the central Lys^{27} in KTX and the C$^\beta$ atoms of Tyr^{375} in the GYGD motive was exploited (6, 21). The docking configuration and the distances between interacting amino acids were analyzed using RasMol 2.7.1.

RESULTS

To initially characterize the effect of extracellularly applied KTX on current through *m*Kv1.1 channels, we measured whole cell currents in response to depolarizing steps from −80 to +40 mV in the absence and presence of KTX (Fig. 1*A*, *left*). 60 nM KTX (Bachem) added to the external mammalian Ringer solution resulted in a peak current reduction of about 50%. To quantify the KTX affinity of *m*Kv1.1, we measured, in additional experiments, the effect of different KTX concentrations on current through *m*Kv1.1 channels and plotted the normalized peak currents against the applied KTX concentration (Fig. 1*B*, *open triangles*). A Hill equation was fitted to the data with a Hill coefficient of 1, indicating a 1:1 stoichiometry suggesting

TABLE I

K$_d$ values (in nM) of the tested channels and channel mutants with the analyzed peptide toxins and peptide toxin mutants at pH$_o$ 7.4 and 6.2

K$_d$ values without S.E. were revealed by fitting (by eye) a Hill equation to data points for different toxin concentrations, whereas each data point represented the mean ± S.E. of at least four experiments. The other values represent the mean ± S.E. of at least four measurements with one toxin concentration. Also shown is the (K$_d$ pH$_o$ 7.4/K$_d$ pH$_o$ 6.2) ratio.

	K_d at pH$_o$ 7.4	K_d at pH$_o$ 6.2	K_d at pH$_o$ 7.4/ K_d at pH$_o$ 6.2
	nM	*nM*	
Kv1.1			
KTX[a]	62	19	3.3
KTX[b]	10.6 ± 2	3.3 ± 0.5	3.3
D361N Kv1.1			
KTX[a]	272 ± 67	82 ± 12	3.6
E353S Kv1.1			
KTX[a]	94 ± 33	40 ± 12	2.4
H404T Kv1.3			
KTX[a]	0.24	0.10	2.4
KTX[b]	0.059 ± 0.006	0.025 ± 0.004	2.3
CTX	0.25	0.25	1
NTX	5.4	7.7	0.7
KTX$_3$	0.15 ± 0.015	0.17 ± 0.025	0.9
KTX-H34A	0.097 ± 0.008	0.096 ± 0.019	1.0
KTX-H34K	0.017 ± 0.003	0.016 ± 0.006	1.06
KTX-R31A/H34A	0.98 ± 0.1	1.07 ± 0.1	0.91
KTX-K32A	0.24 ± 0.04	0.11 ± 0.03	2.2
KTX-K27Dap	5.4 ± 0.3	1.4 ± 0.04	3.8
KTX-K27Dab	5.6 ± 0.3	3.2 ± 0.3	1.8
KTX-K27ThLys	0.19 ± 0.02	0.08 ± 0.01	2.3
KTX-K27Nle	42	16	2.7
KTX-K27A	79 ± 4	33.7 ± 2.5	2.4
D375A/D376A/H404T Kv1.3			
KTX[b]	0.111 ± 0.01	0.102 ± 0.01	1.1
D375A/H404T Kv1.3			
KTX[b]	0.059 ± 0.006	0.056 ± 0.005	1.05
D376A/H404T Kv1.3			
KTX[b]	0.094 ± 0.012	0.040 ± 0.008	2.4
S378E/H404T Kv1.3			
KTX[b]	0.057 ± 0.003	0.016 ± 0.002	3.5
P377A/S378E/H404T Kv1.3			
KTX[b]	0.064 ± 0.006	0.019 ± 0.002	3.4

[a] KTX from Bachem.
[b] Recombinant KTX.

that one KTX molecule is sufficient to block one *m*Kv1.1 channel. The fit gave a dissociation constant K_d at pH$_o$ 7.4 of 62 nM ($n = 25$), which is in agreement with earlier reports (22). The current reduction by KTX was fully reversible upon washout (data not shown). Application of 60 nM KTX (Bachem) to the bath solution at pH$_o$ 6.2 reduced the current much more than 50% (Fig. 1*A*, *right*). The determination of the KTX affinity of *m*Kv1.1 at pH$_o$ 6.2 was made as for pH$_o$ 7.4 and showed a K_d of 19 nM ($n = 28$). Fig. 1*B* clearly demonstrates that the dose-response curve for KTX at pH$_o$ 6.2 (*open squares*) to block currents through *m*Kv1.1 channels was shifted toward lower concentrations. Therefore, lowering pH$_o$ from 7.4 to 6.2 increased the KTX affinity to *m*Kv1.1 ∼ 3.3 times. The same relationship between K_d pH$_o$ 7.4 and 6.2 was revealed with the recombinantly made KTX which exhibited an ∼4 times higher affinity to *m*Kv1.1 channels compared with KTX from Bachem (Table I) probably because of higher purity of the recombinant KTX.

We wanted to know whether this observed higher KTX affinity of *m*Kv1.1 at low pH$_o$ is caused by protonation of an amino acid in the channel protein or by protonation of a residue in KTX. To rule out effects of His^{355} of the *m*Kv1.1 channel (protonation of His^{355} results in a decrease of the TEA affinity at low pH$_o$ (see Ref. 12)), we tested KTX on *m*Kv1.1 mutant channels with a non-protonatable glycine instead of a histidine at position 355 (H355G/*m*Kv1.1). KTX, however, seemed to bind to this H355G mutant *m*Kv1.1 channel in an irreversible

manner since currents could not be recovered after application of KTX even after wash-out for more than 1 h (data not shown). To avoid possible problems with rundown *versus* block, we tested KTX on H404T mutant *m*Kv1.3 channels. The H404T/*m*Kv1.3 channel also contains no protonatable histidine in the outer pore region (Fig. 2*A*). Instead of the histidine, it has a glycine at the corresponding position 380; the histidine residue of the wt *m*Kv1.3 channel at position 404 (equivalent to position 379 of *m*Kv1.1) is changed to a threonine in this mutant of the channel (Fig. 2*A*). We did identical experiments with KTX from Bachem for H404T mutant *m*Kv1.3 channels as we did for *m*Kv1.1 channels. KTX displayed an increased affinity to H404T mutant *m*Kv1.3 channels at low pH$_o$ despite the absence of protonatable histidines in the outer pore region. The dose-response curve for pH$_o$ 6.2 was shifted toward lower concentrations compared with pH$_o$ 7.4 (Fig. 1*C*) and revealed K_d values of 0.24 nM ($n = 28$) and 0.10 nM ($n = 28$) for pH$_o$ 7.4 and 6.2, respectively.

In order to find out whether voltage-dependent binding of KTX could effect the pH$_o$ dependence of KTX block, we investigated voltage dependence of KTX block on current through H404T mutant *m*Kv1.3 channels (Fig. 3). Crest *et al.* (23) and Mourre *et al.* (24) reported that the KTX block of calcium-dependent potassium channels with large conductance (MaxiK channels) and of voltage-dependent potassium channels is voltage-independent at physiological pH$_o$, but there were no studies testing a possible voltage dependence of KTX block at acid

A

B
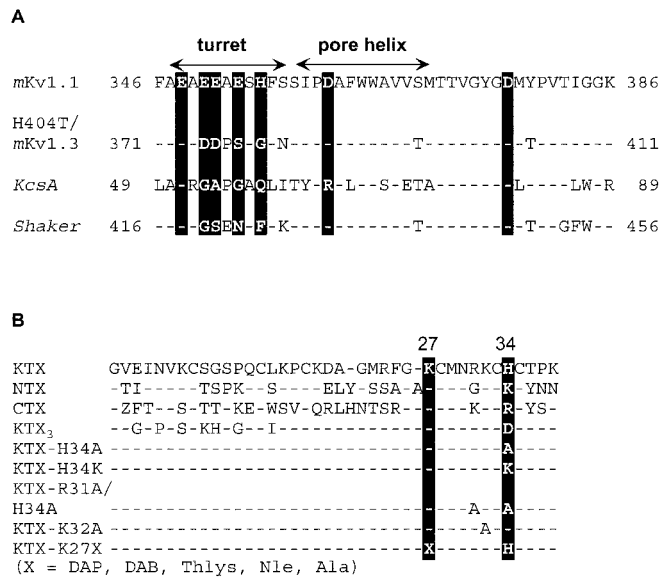
FIG. 2. **Alignment of channels and toxins.** *A*, amino acid alignment of *m*Kv1.1, H404T mutant *m*Kv1.3, *KcsA*, and *Shaker* sequences in the turret and putative pore region. Negatively charged residues of *m*Kv1.1 (Glu[348], Glu[350], Glu[351], Glu[353], Asp[361], Asp[377]) and the corresponding residues in the other channels are highlighted. Also emphasized is His[355] of *m*Kv1.1 (and equivalent positions of the other channels), which was shown to cause pH$_o$ dependence of TEA block (12). *B*, alignment of the amino acid sequences of all investigated peptide toxins and peptide toxin mutants. Highlighted is position 27 of KTX and corresponding residues of the other toxins as well as amino acids at KTX position 34.

pH$_o$. To create a conductance-voltage relationship of the KTX block, we converted the currents shown in Fig. 3 (*A* and *C*) to conductances by dividing the peak currents through the driving force for [K⁺] ($E − E_K$). At pH$_o$ 7.4 application of 50 pM recombinant KTX reduced maximum conductance to 68% of the values obtained in the absence of KTX without changing activation of the channels. The suppression of the conductance was identical at membrane potentials more positive than 0 mV up to +100 mV, indicating that the KTX block on H404T mutant *m*Kv1.3 channels was voltage-independent in that potential range at physiological pH$_o$. At pH$_o$ 6.2, application of 50 pM recombinant KTX reduced maximum conductance $g_{K(max)}$ significantly higher compared with pH$_o$ 7.4 to only 40% of the control value. The KTX block was again voltage-independent; membrane potentials more positive than +20 mV did not modify the blocking strength of KTX (Fig. 3*D*). Since the KTX effect seemed to be independent of the applied voltage for depolarizations between 0 and +100 mV at both pH$_o$ values, it seemed sufficient for later experiments to evaluate the KTX block at one potential, in our case +40 mV, using the ratios of the peak currents (see also Fig. 1*C*). In comparison to the voltage independence of KTX block on current through H404T/*m*Kv1.3 shown here, CTX block of Ca²⁺-activated K⁺ channels (25) and of voltage-dependent *Shaker* K⁺ channels (26) was reported to be slightly voltage-dependent. Both Figs. 1*C* and 3 demonstrate that KTX block on current through H404T mutant *m*Kv1.3 channels was better at low pH$_o$ with a ratio of 237 K_d pH$_o$ 7.4/K_d pH$_o$ 6.2 253 of 2.4 but to a lesser extent compared with *m*Kv1.1 channels with a ratio of 3.3 (Table I). This difference might be explained by distinct amino acids in the outer pore region of *m*Kv1.1 and *m*Kv1.3 channels (for details see below). The existence of a pH$_o$-dependent KTX block of H404T/*m*Kv1.3 channels lacking histidine residues in the pore region indicated that protonation of an amino acid in KTX might be responsible for the higher affinity at low pH$_o$. In all tested channels recombinant KTX blocked current more efficiently compared with

KTX from Bachem (Table I). However, both batches of peptide toxins exhibited a similar pH$_o$ dependence of block with an improvement of the KTX affinity to H404T mutant *m*Kv1.3 of ~2.4 times with changing pH$_o$ from 7.4 to 6.2 (Table I).

To find out further indications for our hypothesis that protonation of an amino acid in KTX is responsible for the higher affinity at pH$_o$ 6.2, we investigated the pH$_o$ dependence of block by other peptide toxins like CTX and NTX on current through the H404T mutant *m*Kv1.3 channels. CTX blocked the current through H404T/*m*Kv1.3 with equal strength at pH$_o$ 7.4 as well as at pH$_o$ 6.2, which can be seen by the identical K_d values shown in Table I for pH$_o$ 7.4 (0.25 nM; n = 28) and pH$_o$ 6.2 (0.25 nM; n = 22). In addition, H404T mutant *m*Kv1.3 channels showed a slight but opposite pH$_o$ dependence of NTX block with K_d values of 5.4 nM (n = 24) and 7.7 nM (n = 20) at pH$_o$ 7.4 and 6.2, respectively (Table I). We therefore concluded that the increase in affinity by lowering pH$_o$ is specific for KTX since CTX and NTX did not show this behavior.

By comparing the amino acid sequence of the toxins, we found that KTX possesses a unique histidine at position 34 not present in CTX and NTX (Fig. 2*B*). In order to find out whether His[34] might be the protonatable amino acid in KTX, we used KTX$_3$ which has an Asp at position 34 whose protonation should not vary between pH$_o$ 7.4 and 6.2. KTX$_3$ exhibited nearly the same affinity to H404T mutant *m*Kv1.3 channels at pH$_o$ 7.4 and 6.2 with K_d values of 150 ± 15 pM (n = 6) and 170 ± 25 pM (n = 6) at pH$_o$ 7.4 and 6.2, respectively (Table I). The loss of the pH$_o$-dependent KTX effect in KTX$_3$ indicated that His[34] of KTX might be responsible for this effect because of the lack of a histidine residue at position 34 in KTX$_3$.

Additional experiments with KTX-Lys[27] mutants on H404T mutant *m*Kv1.3 channels were made to exclude Lys[27] of KTX as the protonatable amino acid of KTX. The KTX mutants K27Dap, K27Dab, and K27ThLys contained non-natural positively charged lysine analogs of varying side chain lengths (Dap, 2.5 Å from C$^\alpha$; Dab, 3.8 Å; ThLys, 7.7 Å; natural lysine, 6.3 Å), whereas in K27A and K27Nle the neutral alanine and the non-natural neutral norleucine replaced lysine (6, 9). If Lys[27] was somehow involved in the pH$_o$ dependence of KTX block, we would expect a pH$_o$-independent block with the non-charged amino acids at position 27 and perhaps an altered pH$_o$ dependence with the shorter and longer non-natural lysine analogs Dap, Dab, and ThLys. Table I shows that all KTX-Lys[27] mutants bound in a pH$_o$-dependent manner to H404T mutant *m*Kv1.3 channels with a higher affinity at low pH$_o$, revealing that Lys[27] is not responsible for pH$_o$ dependence of KTX block.

To further substantiate that protonation of His[34] in KTX is responsible for the pH$_o$ dependence of KTX block on current through *m*Kv1.1 and H404T mutant *m*Kv1.3 channels, we made mutants of this peptide toxin by recombinant methods (17). His[34] of KTX seemed to be a good candidate for the protonatable amino acid in KTX, as indicated by the investigations with H404T/*m*Kv1.1 channels and CTX, NTX, and KTX$_3$. Therefore, we investigated the KTX mutants H34A and H34K. In addition, we also replaced Arg[31] and Lys[32] in KTX with neutral amino acids to examine whether these two positions in KTX were also involved since earlier work indicated that these two positions participate in important interactions (9, 27). We therefore tested the pH$_o$ dependence of block of all four KTX mutants with H404T mutant *m*Kv1.3 channels (Table I). The KTX mutant K32A still had a weaker blocking effect at pH$_o$ 7.4 compared with pH$_o$ 6.2 by a factor of about 2.1 on H404T mutant *m*Kv1.3 channels, suggesting that Lys[32] in KTX did not cause the pH$_o$ dependence of block (Table I). In contrast, KTX-H34A blocked H404T mutant *m*Kv1.3 with the same potency at
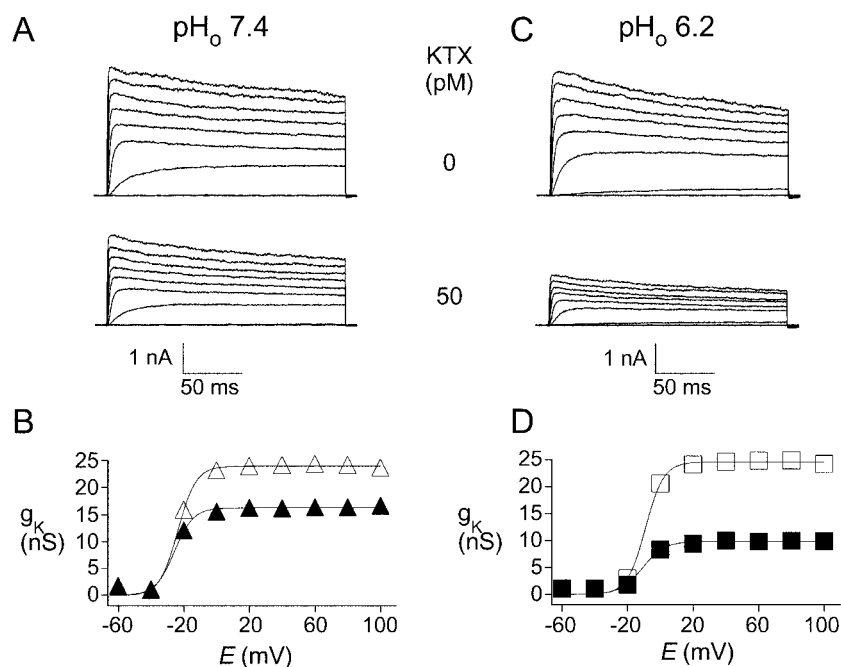
FIG. 3. **Voltage dependence of KTX block on current through H404T mutant *m*Kv1.3 channels at pH$_o$ 7.4 and 6.2.** *A*, currents elicited by a set of 200-ms voltage steps from a holding potential of -80 mV to voltages between -60 and $+100$ mV in 20-mV increments every 20 s, in the absence (*top*) and the presence (*bottom*) of 50 pM recombinantly produced KTX at pH$_o$ 7.4. *B*, corresponding conductances for the currents shown in *A* are plotted against the applied membrane potential, in the absence ($\triangle$) and in the presence ($\blacktriangle$) of KTX. The lines through the points were fitted by a Boltzmann equation: $g_{K(E)} = g_{K(max)}/\{1 + \exp[(E_{1/2} - E)/k]\}$ with values for $g_{K(max)}$ of 24 and 16 nS without and with KTX, respectively. The determined values for k (6 mV) and $E_{1/2}$ (-24 mV) were confirmed by additional experiments. *C*, currents, elicited as described in *A* at pH$_o$ 6.2. *D*, corresponding conductance-voltage relations for the currents shown in *C*, in the absence ($\square$) and in the presence ($\blacksquare$) of KTX. The Boltzmann fit was made as described in *B* with values for $g_{K(max)}$ of 25 and 10 nS without and with KTX, respectively. Values for k (6 mV) and $E_{1/2}$ (-10 mV) were also confirmed by additional experiments.

pH$_o$ 7.4 and 6.2 (Fig. 4*A* (*top*) and Table I). Additional replacement of Arg[31] with alanine in the H34A/R31A mutant KTX exhibited no further effect (Table I). Replacement of His[34] in KTX by lysine led to the same effect as substitution by alanine concerning the pH$_o$-independent block but exhibited a higher affinity to H404T/*m*Kv1.3 than H34A and wt KTX (Fig. 4*A* (*bottom*) and Table I). Therefore H34A, H34K, and R31A/H34A mutants of KTX blocked currents through H404T mutant *m*Kv1.3 channels in a pH$_o$-independent manner, whereas KTX-K32A block is influenced by pH$_o$. These results suggest that only the histidine residue at position 34 of KTX is the protonatable amino acid of KTX that causes pH$_o$ dependence of block while Arg[31] and Lys[32] of KTX do not seem to play a role in this effect.

If protonation of His[34] in KTX is the reason for the better block of *m*Kv1.1 and H404T mutant *m*Kv1.3 channels with lowering pH$_o$, H34A and H34K mutants of KTX should (*a*) have a pH$_o$-independent block as shown before (Fig. 4*A* and Table I) and (*b*) represent the fully protonated (H34K) and the fully unprotonated (H34A) form of wt KTX responsible for the pH$_o$ dependence of block. Fig. 4*B* shows the titration of wt KTX and the mutants H34K and H34A from pH$_o$ 5.5 to pH$_o$ 7.8 examined on H404T mutant *m*Kv1.3 channels. KTX-H34K exhibited the same K_d of $\sim$16 pM in the investigated pH$_o$ range, and KTX-H34A had identical K_d values of $\sim$100 pM at 6 different pH$_o$ values between pH$_o$ 5.5 and 7.4. Linear regressions through the data points of both KTX mutants had slopes of zero, indicating that these KTX mutants cannot be titrated in the pH$_o$ range used. This also suggests that histidine at position 34 of KTX is protonatable. The affinity of wt KTX to H404T mutant *m*Kv1.3 channels decreased with increasing pH$_o$. The fit through the data points using the Hill equation gave a $K_{d(min)}$ of 18 pM at pH$_o$ 5.5 and a $K_{d(max)}$ of 60 pM at pH$_o$ 7.8 and a pK_a of 6.5, which represents the pH of the half-maximum protonation. The Hill

coefficient of 1.7 suggests that more than one negatively charged amino acids of the channel protein could sense His[34] of KTX. The $K_{d(min)}$ of 18 pM wt KTX at pH$_o$ 5.5 is the expected value with good agreement with the K_d of KTX-H34K, which stands for the fully protonated form of wt KTX. In contrast, KTX-H34A, which represents the unprotonated wt KTX, had a lower affinity to H404T/*m*Kv1.3 channels with 100 pM compared with $K_{d(max)}$ of wt KTX with 60 pM at pH$_o$ 7.8. The reason for this difference might be a non-ionic interaction between the unprotonated His[34] of wt KTX and an amino acid of the channel that is abolished by the substitution with alanine. A more conservative replacement with glutamine or asparagine might solve this question (28, 29). Since the data confirmed our predictions apart from this difference between $K_{d(max)}$ of wt KTX and K_d of KTX-H34A, we concluded that indeed protonation of His[34] in KTX caused the pH$_o$ dependence of block.

To determine which amino acid(s) of the channel protein interacted with the protonatable His[34] of KTX, we tested some mutants of the *m*Kv1.1 and the H404T/*m*Kv1.3 channels, respectively. Six negatively charged residues in the *m*Kv1.1 pore region could be candidates for the interaction with His[34] in KTX: Glu[348], Glu[350], Glu[351], Glu[343], Asp[361], and Asp[377] (Fig. 2*A*). The *m*Kv1.3 channel contains all of these negatively charged amino acids except one at position 378, which corresponds to position 353 of *m*Kv1.1 with an uncharged serine instead of the glutamate in *m*Kv1.1. We did not investigate the Asp[377] of *m*Kv1.1 (Asp[402] in *m*Kv1.3) of the GYGD motif, since we had found that the shorter lysine analogs Dap and Dab at position 27 of KTX that were shown to interact with Asp[402] in *m*Kv1.3 (6) still blocked in a pH$_o$-dependent manner (Table I). In addition, from the *KcsA* crystal structure data, we concluded that the negative charges at positions 348–353 of *m*Kv1.1 would be the best candidates for the interacting amino acids. We expected that replacing negatively charged amino acids in

Mammalian K^+ Channel Structure

H404T mutant *m*Kv1.3

A

pH_o 7.4   **pH_o 6.2**

control
KTX-H34A

control
KTX-H34A

200 pA |__|
50 ms

200 pA |__|
50 ms

control
KTX-H34K

control
KTX-H34K

200 pA |__|
50 ms

200 pA |__|
50 ms

B

K_d
(pM)

▲ KTX-H34A

□ wt KTX

● KTX-H34K

pH_O
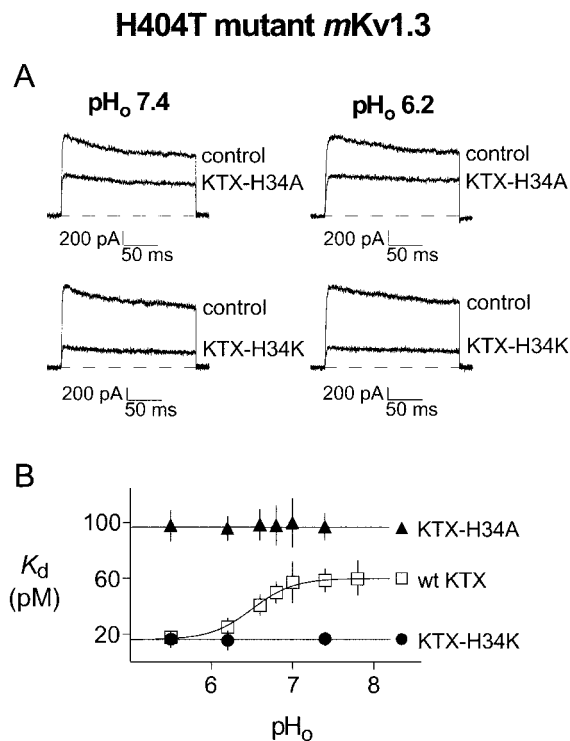
FIG. 4. **pH_o dependence of block of recombinant wt KTX and the KTX mutants H34A and H34K on current through H404T mutant mKv1.3 channels.** *A*, pH_o-independent block of KTX mutants H34A (*top*) and H34K (*bottom*). Currents were elicited as described in the legend to Fig. 1*A*. *B*, Mean K_d values and standard deviations of wt KTX (□), KTX-H34A (▲), and KTX-H34K (●) block of current through H404T mutant *m*Kv1.3 channels were plotted against the pH_o. K_d values were obtained as described in the legend to Fig. 1*A*. The curve through the wt KTX data points represents a fit with the equation $K_d = K_{d(max)} + \{[K_{d(max)} - K_{d(min)}]/[1 + (10^{pH_o}/10^{pKa})^h]\}$ with $K_{d(max)}$ of 60 pM, $K_{d(min)}$ of 18 pM, pK_a of 6.5, and a Hill coefficient, *h*, of 1.7. The applied wt KTX was made recombinantly. Straight lines through data points for KTX-H34A and KTX-H34K represent linear regressions with slopes of zero.

the channel that interact with His[34] with neutral residues would diminish or abolish pH_o-dependent KTX block, depending on whether the negatively charged residue alone or together with others could sense His[34] in KTX. As a starting point, we investigated Glu[353] of *m*Kv1.1 as an interacting residue because of the dissimilar amino acid at the equivalent position of H404T/*m*Kv1.3 channels, which might explain the different ratios (K_d pH_o 7.4/K_d pH_o 6.2) of both channels. The E353S mutant *m*Kv1.1 channel showed still an improvement of KTX affinity with lowering pH_o with K_d values of 94 nM and 40 nM (*n* = 5) for pH_o 7.4 and 6.2, respectively (Table I). Nevertheless, the ratio of (K_d pH_o 7.4/K_d pH_o 6.2) was reduced to 2.4, the same ratio as for H404T mutant *m*Kv1.3 channels. Therefore, we concluded that (*a*) the lack of a negative charge at position 378 in *m*Kv1.3 (equivalent to 353 in *m*Kv1.1) reduced the (K_d pH_o 7.4/K_d pH_o 6.2) ratio, and (*b*) that Glu[353] in *m*Kv1.1 is one of the negatively charged residues in *m*Kv1.1, which interacts with the protonatable amino acid in KTX. This result was confirmed by the introduction of a negatively charged amino acid at *m*Kv1.3 position 378 (P377A/S378E/H404T and S378E/H404T mutant *m*Kv1.3 channels) exhibiting the stronger improvement of KTX block with lowering pH_o like *m*Kv1.1 channels (Table I). Therefore, protonation of His[355] in *m*Kv1.1 (12) seemed not to cause the stronger pH_o effect of *m*Kv1.1 compared with H404T/*m*Kv1.3.

As additional candidate for an interacting amino acid of the channel, we investigated the D361N mutant *m*Kv1.1 channel

lacking the negative charge at position 361 (equivalent to position 386 in *m*Kv1.3). As can be seen from Table I, despite the deficiency in this negative charge, KTX block is still pH_o-dependent and exhibited the same (K_d pH_o 7.4/K_d pH_o 6.2) ratio as wt *m*Kv1.1. Therefore we concluded that Asp[361] in *m*Kv1.1 (Asp[386] in *m*Kv1.3) did not interact with His[34] in KTX.

Furthermore, we investigated whether the negative charges in *m*Kv1.1 position 350 and 351 (corresponding to positions 375 and 376 in *m*Kv1.3) sense the protonatable His[34] in KTX. These studies were performed with three mutants of the H404T/*m*Kv1.3 channel since equivalent *m*Kv1.1 mutants could not be expressed in RBL cells. Substitution of both negatively charged aspartate residues with neutral alanines in the D375A/D376A/H404T mutant *m*Kv1.3 channel diminished the pH_o dependence of KTX block (Table I). Since we could not detect any statistical significant difference between the K_d values at pH_o 7.4 and 6.2 by using Student's *t* test ($p < 0.05$), removal of the negative charges at position 375 and 376 in *m*Kv1.3 abolished the pH_o dependence of KTX block. To test whether both or only one of these glutamates could interact with His[34] in KTX, we replaced only one of the negative charged residues by a neutral alanine. The D376A/H404T mutant *m*Kv1.3 channels showed the same pH_o-dependent KTX block as H404T/*m*Kv1.3 channels with an unchanged (K_d pH_o 7.4/K_d pH_o 6.2) ratio of 2.4 (Table I). In contrast, KTX displayed the same affinity to D375A/H404T mutant *m*Kv1.3 channels at pH_o 7.4 and 6.2 with an identical (K_d pH_o 7.4/K_d pH_o 6.2) ratio to D375A/D376A/H404T mutant *m*Kv1.3 channels. Again there was no statistical significant difference between the K_d values at pH_o 7.4 and 6.2 analyzed with Student's *t* test with $p < 0.05$; accordingly, we concluded that only Asp[375] interacts with the protonatable His[34] in KTX. From this result we could also exclude Glu[373] in *m*Kv1.3 and the equivalent Glu[348] in *m*Kv1.1 to interact with His[34] in KTX.

To calculate the distances between His[34] in KTX and Glu[353]/Glu[350] in *m*Kv1.1, we performed electrostatic compliance. Protonation of His[34] in KTX caused a higher effective KTX concentration of 200 nM at pH_o 6.2 compared with the bulk concentration of 60 nM. The raised effective KTX concentration was due to the interaction of both Glu[353] and Glu[350] with His[34]/KTX. E353S mutant *m*Kv1.1 channels exhibited the exclusive interaction between Glu[350]/*m*Kv1.1 and His[34]/KTX with an effective KTX concentration of 235 nM at pH_o 6.2 in contrast to the bulk concentration of 100 nM. The sole interaction between Glu[353]/*m*Kv1.1 and His[34]/KTX was calculated by dividing the K_d factor for *m*Kv1.1 by the same factor for E353S/*m*Kv1.1, indicating that protonation of His[34]/KTX would raise KTX concentration 1.4 times due to the interaction with Glu[353] in *m*Kv1.1.

The knowledge about the effective KTX concentration enabled us to determine the potential ψ, which caused the higher effective KTX concentration at low pH_o. ψ for wt *m*Kv1.1 was −30.4 mV, for E353S/*m*Kv1.1 −22 mV, and for the calculated mutant E350A/*m*Kv1.1 −8.6 mV. These values for ψ were correct if only one Glu[350] and Glu[353], respectively, of the channel would sense protonation of His[34] in KTX. Because it was not possible to determine the number of interacting channel subunits without investigating heterotetrameric channels, we calculated the potentials for one, two, and four interacting channel subunits by dividing the above ψ values by these numbers of subunits. Because of the distance dependence of electrostatic interactions, we were able to determine the distance between interacting amino acids of *m*Kv1.1 and KTX. For this calculation the degree of charge that was caused by protonation of His[34] has to be known and was calculated with 67% protonation at pH_o 6.2 (12). We estimated distances of 4, 6–6.5, or 8.5

Å between His[34]/KTX and one, two, or four interacting Glu[350]/
*m*Kv1.1 and distances of 6.5–7, 9.5, or 12.5 to 14 Å between
His[34]/KTX and one, two, or four interacting Glu[353]/*m*Kv1.1.

Corresponding calculations were performed for interacting
residues in H404T/*m*Kv1.3 and His[34] in KTX. We estimated the
same distances for His[34]/KTX and Asp[375]/*m*Kv1.3 as for His[34]/
KTX and Glu[350]/*m*Kv1.1. The distance between His[34]/KTX and
S378E/*m*Kv1.3 also seemed to be the same as for His[34]/KTX
and Glu[353]/*m*Kv1.1.

Furthermore, we calculated the distance between the only
interacting residue in H404T/*m*Kv1.3 channels, Asp[375], and
His[34]/KTX by electrostatic compliance using KTX₃ and KTX-
H34K. By application of the known charge difference of two
between Asp[34] in KTX₃ and Lys[34] in H34K (Fig. 2) and the K_d
values (Table I), we calculated a local potential 89 of −55.9 mV.
Therefore, we found distances between Asp[375]/*m*Kv1.3 and
His[34]/KTX of 4–4.5 Å for the interaction with one channel
subunit, of 6.5–7 Å for the interaction with two subunits, and of
9 Å for the interaction with all four channel subunits, respec-
tively. The agreement of this electrostatic compliance calcula-
tion using the known charge difference between H34K and
KTX₃ at position 34 with the electrostatic compliance using the
degree of protonation at His[34]/KTX enabled us to confirm the
above determined pK_a of His[34]/KTX.

Estimation of the distance between Asp[375]/*m*Kv1.3 and
His[34]/KTX was also carried out by mutant cycle analysis. The
KTX block of the channel mutants D375A/H404T and D375A/
H404T was tested at pH$_o$ 7.4 and 6.2 (Table I) using the
different degrees of protonation at KTX position His[34] instead
of mutations at KTX position 34. The change in coupling energy
$\Delta\Delta G$ of 0.5 kcal mol^{-1} indicated a distance of maximally 5 Å
between Asp[375] of *m*Kv1.3 and His[34] of KTX (7, 20). The mu-
tant cycle analysis confirmed the distance calculation by elec-
trostatic compliance and suggested the interaction of His[34]/
KTX with Asp[375] in only one channel subunit.

To refine the docking conformation of *m*Kv1.1 with KTX, we
confirmed the known interacting pair of Gly[380]/Kv1.3 and
Arg[31]/KTX for the *m*Kv1.1 channel (9). We investigated wt and
H355K mutant *m*Kv1.1 channels with the KTX mutants H34A
versus R31A/H34A. wt *m*Kv1.1 exhibited an ~10 times higher
affinity to H34A compared with R31A/H34A with K_d values of
38 ± 4 n*M* and 410 ± 40 n*M*, respectively. In contrast, R31A/
H34A blocked current through H355K mutant *m*Kv1.1 chan-
nels only 2 times more weakly than the H34A mutant KTX
with K_d values of 1120 ± 180 n*M* and 620 ± 80 n*M* for R31A/
H34A and H34A block, respectively. Application of mutant
cycle analysis revealed a $\Delta\Delta G$ value of 1.05 kcal mol^{-1}, which
indicates a proximity of ≤5 Å between the interacting residues
His[355] in *m*Kv1.1 and Arg[31] in KTX similar to the Kv1.3-KTX
complex.

Using a homology model of the *m*Kv1.1 channel based on the
known crystal structure of the *KcsA* channel (8), we visualized
the docking configuration of *m*Kv1.1 and KTX. The docking of
KTX into the *m*Kv1.1 homology model is shown in Fig. 5. KTX
is shown in *green*, *m*Kv1.1 in *gray*. The interacting amino acids
of channel and toxin (Arg[31] and His[34] of KTX and Glu[350],
Glu[353], and His[355] of *m*Kv1.1) are drawn as Corey-Pauling-
Koltun surfaces, the remaining channel as *schematic*, the re-
maining toxin as *ribbon*. His[34] of KTX interacts with Glu[350]
and Glu[353] of one channel subunit as indicated by the mutant
cycle analysis between Asp[375]/*m*Kv1.3 and His[34]/KTX. The
large distances between two adjacent or opposite channel sub-
units would not yield the interaction strength measured by
electrostatic compliance and mutant cycle analyses. The dock-
ing of KTX into the *m*Kv1.1 homology model based on the *KcsA*
structure was performed using the interactions between chan-
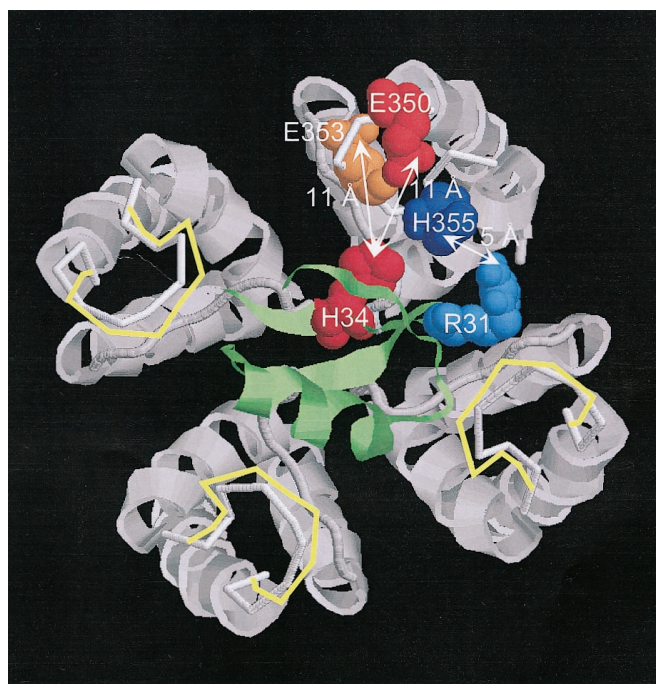
FIG. 5. **Docking of KTX into a homology model of *m*Kv1.1.** The
docking configuration is shown as top view. The homology structure of
*m*Kv1.1 based on the *KcsA* crystal structure. The channel backbone is
shown in *gray* as a *schematic*, KTX is shown in *green* as *ribbons*.
Selected side chains are shown as Corey-Pauling-Koltun surfaces with
Glu[350]/*m*Kv1.1 in *red-orange*, Glu[353]/*m*Kv1.1 in *orange*, His[34]/KTX in
red, His[355]/*m*Kv1.1 in *dark blue*, and Arg[31]/KTX in *blue*. Distances
between interacting amino acids of *m*Kv1.1 and KTX suggested by the
docking are given in *white*. The *yellow line* simulates the position of the
turret in *m*Kv1.1, as suggested by the experimentally derived distances
between Glu[350] and Glu[353] in *m*Kv1.1 and His[34] in KTX. The arrange-
ment of the simulated turret was made by rotating the backbone of the
turret toward the center of the pore. The figure was made using RasMol
2.7.1.

nel and toxin described here and, additionally, the interaction
between Tyr[375]/*m*Kv1.1 and Lys[27]/KTX (6). The docking exhib-
ited distances of 11 Å between Glu[350]/*m*Kv1.1 and His[34]/KTX,
of 11 Å between Glu[353]/*m*Kv1.1 and His[34]/KTX, and of 5 Å
between His[355]/*m*Kv1.1 and Arg[31]/KTX. Therefore, the docking
distance between Glu[350]/*m*Kv1.1 and His[34]/KTX was 7 Å and
between Glu[353]/*m*Kv1.1 and His[34]/KTX 4–4.5 Å larger com-
pared with the experimentally determined distances. The dock-
ing distance of 5 Å between His[355]/*m*Kv1.1 and Arg[31]/KTX was
identical to the distance calculated by mutant cycle analysis
according to the experimental results. The docking suggested
distances of 22 Å between Glu[350]/*m*Kv1.1 and of 15 Å between
Glu[353]/*m*Kv1.1 and the center of the pore. In contrast, the
experimentally derived results indicated distances of 15 Å be-
tween Glu[350] and of 10.5–11 Å between Glu[353] in *m*Kv1.1 and
the pore axis. The *m*Kv1.1 homology model has the same amino
acid sequence compared with the *m*Kv1.1 clone, but the struc-
ture of the protein backbone was identical to *KcsA*. Therefore,
deviations between the experimentally determined distances
and the docking distances might indicate a different spatial
arrangement of the turret in *m*Kv1.1 and *KcsA* (amino acids
348–357 in *m*Kv1.1). Guiding the turret at position 350 7 Å and
at position 353 4–4.5 Å more toward the center of the pore as
simulated by the *yellow line* in Fig. 5 would match experimen-
tally determined and docking distances. To satisfy our data, we
must modify the *KcsA* crystal structure for *m*Kv1.1, which
suggests structural differences between *m*Kv1.1 and *KcsA* in
the outer pore region. Since *m*Kv1.3 exhibited the same inter-
acting positions and interaction strengths in the turret like
*m*Kv1.1, the *m*Kv1.3 structure might differ from *KcsA* as well.

*m*Kv1.1 and *m*Kv1.3 and maybe other mammalian voltage-gated potassium channels seem to be structurally different from *KcsA* in the turret.

DISCUSSION

In this report we demonstrate that the pH$_o$ dependence of KTX block on current through *m*Kv1.1 and H404T mutant *m*Kv1.3 channels is caused by protonation of the histidine at KTX position 34. We could define two interacting positions of the channel proteins: 350/353 in *m*Kv1.1 and 375/378 in H404T mutant *m*Kv1.3 channels, respectively. Furthermore, we could confirm an equivalent interaction between Arg[31] in KTX and His[355] in *m*Kv1.1 known for Kv1.3 and KTX (9). Comparing experimentally derived and docking distances between interacting residues of *m*Kv1.1 and KTX indicated that the turret of *m*Kv1.1 is oriented more toward the center of the pore compared with *KcsA* whose structure was used as template for the *m*Kv1.1 homology model. In summary, we present new pairs of interacting residues between KTX and the potassium channels *m*Kv1.1 and *m*Kv1.3 to increase the knowledge about the outer pore region of these channels, which might be advantageous in designing novel drugs of higher affinity and specificity.

This is the first report of a peptide toxin binding to potassium channels whose affinity to the channel's receptor was increased in low pH$_o$. Deutsch *et al.* (10) reported about an enhanced CTX binding to the voltage-gated K$^+$ channel in human T lymphocytes with increasing pH$_o$. The reduced CTX and KTX block of wt Kv1.3 in acid pH$_o$ was shown to be a consequence of protonation of His[404] in wt Kv1.3 channels, which repelled the positively charged toxins (9). Replacing His[404] in Kv1.3 with non-protonatable threonine caused a pH$_o$-independent CTX block and an increased KTX block corresponding to our results (9). The diminished CTX block of F425H mutant *Shaker* channels at low pH$_o$ was also a result of protonation of F425H of this *Shaker* mutant (11). Diminished sensitivity of tityustoxin to the squid potassium channel SqKv1A was also attributed to the protonation of a histidine at position 351 (equivalent to *Shaker* position 425) of the channel (14).

Other blocking agents like TEA also exhibited a pH$_o$ dependence of block. Diminished TEA block on current through *m*Kv1.1 channels was caused by protonation of His[355] in *m*Kv1.1, which induced an electrostatic repulsion of the positively charged TEA (12). Weaker sensitivity of saxitoxin and tetrodotoxin to block voltage-gated sodium channel at low pH$_o$ was also discussed to be a result of protonation of the receptor (1, 13), but there is also evidence that the decreased block with increasing [H$^+$]$_o$ or increasing concentration of di- or trivalent cations is caused by neutralization of negative surface charges lowering the saxitoxin and tetrodotoxin concentration at its receptor site (30).

The reduced blocking strength of the above toxins was caused by protonation of the receptor or by changing the surface potentials. None of these examples revealed altered affinity because of protonation of the blocker itself. Therefore, our observations regarding the pH$_o$ dependence of KTX block are different in two respects. First, the KTX block of *m*Kv1.1 and H404T mutant *m*Kv1.3 channels is increased with decreasing pH$_o$. Second, this higher affinity is the result of protonation of an amino acid in the peptide toxin, whereas protonation of the KTX receptor seemed not to play a role in causing this effect.

pH$_o$ independence of CTX and KTX$_3$ block on current through H404T/*m*Kv1.3 indicated that protonation of His[34]/KTX could cause the pH$_o$ dependence of KTX block. Our hypothesis was proven by the pH$_o$-independent KTX-H34A and KTX-H34K block. Titration of wt and mutant KTX revealed that H34K behaved like the fully protonated wt KTX. On the other hand, H34A, which should behave like fully unproto-

nated wt KTX, certainly blocked H404T/*m*Kv1.3 in a pH$_o$-independent manner, however, with a lower affinity compared with wt KTX at pH$_o$ 7.8 with a degree of protonation less than 5%. The difference in affinity between wt KTX at high pH$_o$ and H34A might be caused by an interaction between His[34]/KTX and residues of the channel via the nitrogen atoms, which is destroyed by the substitution with alanine. More conservative exchanges of His[34] with glutamine or asparagine might have the same blocking strength as unprotonated wt KTX, as shown for several histidine interactions in other proteins (28, 29).

Titration of wt KTX also indicated a pK_a of 6.5 for His[34]/KTX. Gairi *et al.* (27) determined the pK_a of His[34] in unbound KTX by NMR investigations with a value of about 5.2. These two observations seem to be in contrast; however, we investigated the pK_a of KTX that was interacting with H404T/*m*Kv1.3 channels and not while unbound in solution. The stronger interaction of protonated His[34]/KTX with negatively charged residues of the H404T channel might facilitate the protonation of His[34] and therefore raise its pK_a. Similar observations with lowered pK_a values (20) and elevated pK_a values (31) due to unfavorable and advantageous interactions with the receptor or ligand have been reported previously.

Replacing negatively charged residues in the outer pore vestibule of *m*Kv1.1 and H404T/*m*Kv1.3 or *vice versa* revealed Glu[350] and Glu[353] in *m*Kv1.1 and Asp[375] in H404T to sense protonation of His[34] in KTX. Since *m*Kv1.1 and *m*Kv1.3 exhibited the same interacting positions and the same strength of interaction, we could transfer results from one channel to the other. Using electrostatic compliance we were able to calculate the distances between the interacting residues of the KTX and both channels (5, 9). Application of two mutant cycles refined the docking configuration of KTX and suggested that His[34]/KTX interacted with only one subunit of the channel.

We used these experimental data for a docking of KTX into a *m*Kv1.1 homology model based on the *KcsA* coordinates (8). The average sequence identity of about 30% between *KcsA* and *m*Kv1.1 is sufficient to generate homology models using the *KcsA* structure as template (32). The docking of KTX into the *m*Kv1.1 homology model built on the basis of the *KcsA* structure exhibited a distance of about 5 Å between His[355]/*m*Kv1.1 and Arg[31]/KTX, which agrees with the experimentally derived distance. The pore diameter of about 30 Å at position 355/*m*Kv1.1 corresponds to the equivalent positions in Kv1.3 and *Shaker* channels (9, 19). In contrast, the docking distances at *m*Kv1.1 positions 350 and 353 within the turret disagreed from the experimentally obtained distances, suggesting shorter pore diameter at these positions for *m*Kv1.1 compared with *KcsA*. To get an agreement between the experimental and the docking data, we would have to modulate the *KcsA* structure within the turret (amino acids 348–357) guiding Glu[350] 7 Å and Glu[353] 4–4.5 Å more toward the center of the pore. Therefore, the shape of the *m*Kv1.1 turret seemed to be distinct from *KcsA*, particularly in the region near the S5 segment but not in the region close to the pore helix. The spatial arrangement of the turret in *m*Kv1.3 and *m*Kv1.1 seems to be very similar since we found identical interacting positions and the same distances between the interacting positions. Evidence for topological differences between *KcsA* and voltage-gated potassium channels within the turret is also indicated by distinct toxin affinities of both channel types (33, 34). Only the replacement of the complete outer pore region of *KcsA* with the equivalent region of a mammalian voltage-gated potassium channel could create a similar toxin affinity in *KcsA* (35).

In conclusion, using KTX as a molecular caliper, we were able to characterize topological features within the turret of the voltage-gated potassium channels *m*Kv1.1 and *m*Kv1.3. The

turret of both channels seems to be structurally different compared with the bacterial *KcsA* channel. Since the receptor for many potassium channel modulators is located in the outer pore region, this information could aid the rational drug design and therefore accelerate the generation of new and improved drugs working on potassium channel.

REFERENCES

1. Hille, B. (1992) *Ionic Channels of Excitable Membranes*, 2nd Ed., Sinauer Associates, Sunderland, MA
2. Miller, C. (1995) *Neuron* **15,** 5–10
3. MacKinnon, R., Heginbotham, L., and Abramson, T. (1990) *Neuron* **5,** 767–771
4. MacKinnon, R. (1991) *Nature* **350,** 232–235
5. Stocker, M., and Miller, C. (1994) *Proc. Natl. Acad. Sci. U. S. A.* **91,** 9509–9513
6. Aiyar, J., Rizzi, J. P., Gutman, G. A., and Chandy, K. G. (1996) *J. Biol. Chem.* **271,** 31013–31016
7. Rauer, H., Lanigan, M. D., Pennington, M. W., Aiyar, J., Ghanshani, S., Cahalan, M. D., Norton, R. S., and Chandy, K. G. (2000) *J. Biol. Chem.* **275,** 1201–1208
8. Doyle, D. A., Cabral, J. M., Pfuetzner, R. A., Kuo, A., Gulbis, J. M., Cohen, S. L., Chait, B. T., and MacKinnon, R. (1998) *Science* **280,** 69–77
9. Aiyar, J., Withka, J. M., Rizzi, J. P., Singleton, D. H., Andrews, G. C., Lin, W., Boyd, J., Hanson, D. C., Simon, M., and Dethlefs, B. (1995) *Neuron* **15,** 1169–1181
10. Deutsch, C., Price, M., Lee, S., King, V. F., and Garcia, M. L. (1991) *J. Biol. Chem.* **266,** 3668–3674
11. Perez-Cornejo, P., Stampe, P., and Begenisich, T. (1998) *J. Gen. Physiol.* **111,** 441–450
12. Bretschneider, F., Wrisch, A., Lehmann-Horn, F., and Grissmer, S. (1999) *Biophys. J.* **76,** 2351–2360
13. Ulbricht, W., and Wagner, H. H. (1975) *Philos. Trans. R. Soc.* **270,** 353–363
14. Dudlak, C. S., Jerng, H. H., and Gilly, W. F. (2000) *Biophys. J.* **78,** 97A
15. Eccleston, E., Leonard, B. J., Lowe, J. S., and Welford, H. J. (1973) *Nat. New Biol.* **244,** 73–76
16. Rauer, H., and Grissmer, S. (1996) *Mol. Pharmacol.* **50,** 1625–1634
17. Garcia, M. L., Hanner, M., Knaus, H. G., Slaughter, R., and Kaczorowski, G. J. (1999) *Methods Enzymol.* **294,** 624–39, 624–639
18. Chandy, K. G., Williams, C. B., Spencer, R. H., Aguilar, B. A., Ghanshani, S., Tempel, B. L., and Gutman, G. A. (1990) *Science* **247,** 973–975
19. Hidalgo, P., and MacKinnon, R. (1995) *Science* **268,** 307–310
20. Schreiber, G., and Fersht, A. R. (1995) *J. Mol. Biol.* **248,** 478–486
21. Kalman, K., Pennington, M. W., Lanigan, M. D., Nguyen, A., Rauer, H., Mahnir, V., Paschetto, K., Kem, W. R., Grissmer, S., Gutman, G. A., Christian, E. P., Cahalan, M. D., Norton, R. S., and Chandy, K. G. (1998) *J. Biol. Chem.* **273,** 32697–32707
22. Grissmer, S., Nguyen, A. N., Aiyar, J., Hanson, D. C., Mather, R. J., Gutman, G. A., Karmilowicz, M. J., Auperin, D. D., and Chandy, K. G. (1994) *Mol. Pharmacol.* **45,** 1227–1234
23. Crest, M., Jacquet, G., Gola, M., Zerrouk, H., Benslimane, A., Rochat, H., Mansuelle, P., and Martin-Eauclaire, M. F. (1992) *J. Biol. Chem.* **267,** 1640–1647
24. Mourre, C., Chernova, M. N., Martin-Eauclaire, M. F., Bessone, R., Jacquet, G., Gola, M., Alper, S. L., and Crest, M. (1999) *J. Pharmacol. Exp. Ther.* **291,** 943–952
25. MacKinnon, R., and Miller, C. (1988) *J. Gen. Physiol.* **91,** 335–349
26. Goldstein, S. A., and Miller, C. (1993) *Biophys. J.* **65,** 1613–1619
27. Gairi, M., Romi, R., Fernandez, I., Rochat, H., Martin-Eauclaire, M. F., Van, R. J., Pons, M., and Giralt, E. (1997) *J. Pept. Sci.* **3,** 314–319
28. Shapiro, R., and Vallee, B. L. (1989) *Biochemistry* **28,** 7401–7408
29. Rehwald, M., Neuschafer-Rube, F., de Vries, C., and Püschel, G. P. (1999) *FEBS Lett.* **443,** 357–362
30. Grissmer, S. (1984) *Pflügers Arch.* **402,** 353–359
31. Loewenthal, R., Sancho, J., and Fersht, A. R. (1992) *J. Mol. Biol.* **224,** 759–770
32. Rodriguez, R., Chinea, G., Lopez, N., Pons, T., and Vriend, G. (1998) *Bioinformatics* **14,** 523–528
33. Garcia, M. L., Garcia-Calvo, M., Hidalgo, P., Lee, A., and MacKinnon, R. (1994) *Biochemistry* **33,** 6834–6839
34. MacKinnon, R., Cohen, S. L., Kuo, A., Lee, A., and Chait, B. T. (1998) *Science* **280,** 106–109
35. Legros, C., Pollmann, V., Knaus, H. G., Farrell, A. M., Darbon, H., Bougis, P. E., Martin-Eauclaire, M. F., and Pongs, O. (2000) *J. Biol. Chem.* **275,** 16918–16924

Structural Differences of Bacterial and Mammalian K$^+$Channels

Anja Wrisch and Stephan Grissmer